



Article

Transport Characteristics of CJMAED™ Homogeneous Anion Exchange Membranes in Sodium Chloride and Sodium Sulfate Solutions

Veronika Sarapulova ¹, Natalia Pismenskaya ¹, Valentina Titorova ¹, Mikhail Sharafan ¹, Yaoming Wang ², Tongwen Xu ², Yang Zhang ³ and Victor Nikonenko ^{1,*}

¹ Membrane Institute, Kuban State University, 149 Stavropolskaya St., 350040 Krasnodar, Russia; vsarapulova@gmail.com (V.S.); n_pismen@mail.ru (N.P.); valentina.titorova@mail.ru (V.T.); shafron80@mail.ru (M.S.)

² CAS Key Laboratory of Soft Matter Chemistry, Collaborative Innovation Center of Chemistry for Energy Materials, School of Chemistry and Material Science, University of Science and Technology of China, Hefei 230026, China; ymwong@ustc.edu.cn (Y.W.); twxu@ustc.edu.cn (T.X.)

³ School of Environmental and Safety Engineering, Qingdao University of Science and Technology, 53 Zhenzhou Road, Qingdao 266042, China; zhangyang@qust.edu.cn

* Correspondence: v_nikonenko@mail.ru; Tel.: +7-918-414-58-16



Citation: Sarapulova, V.; Pismenskaya, N.; Titorova, V.; Sharafan, M.; Wang, Y.; Xu, T.; Zhang, Y.; Nikonenko, V. Transport Characteristics of CJMAED™ Homogeneous Anion Exchange Membranes in Sodium Chloride and Sodium Sulfate Solutions. *Int. J. Mol. Sci.* **2021**, *22*, 1415. <https://doi.org/10.3390/ijms22031415>

Academic Editors: Artur J.M. Valente and Larry Fliegel

Received: 30 December 2020

Accepted: 27 January 2021

Published: 31 January 2021

Publisher's Note: MDPI stays neutral with regard to jurisdictional claims in published maps and institutional affiliations.



Copyright: © 2021 by the authors. Licensee MDPI, Basel, Switzerland. This article is an open access article distributed under the terms and conditions of the Creative Commons Attribution (CC BY) license (<https://creativecommons.org/licenses/by/4.0/>).

Abstract: The interplay between the ion exchange capacity, water content and concentration dependences of conductivity, diffusion permeability, and counterion transport numbers (counterion permselectivity) of CJMA-3, CJMA-6 and CJMA-7 (Hefei Chemjoy Polymer Materials Co. Ltd., China) anion-exchange membranes (AEMs) is analyzed using the application of the microheterogeneous model to experimental data. The structure-properties relationship for these membranes is examined when they are bathed by NaCl and Na₂SO₄ solutions. These results are compared with the characteristics of the well-studied homogenous Neosepta AMX (ASTOM Corporation, Japan) and heterogeneous AMH-PES (Mega a.s., Czech Republic) anion-exchange membranes. It is found that the CJMA-6 membrane has the highest counterion permselectivity (chlorides, sulfates) among the CJMAED series membranes, very close to that of the AMX membrane. The CJMA-3 membrane has the transport characteristics close to the AMH-PES membrane. The CJMA-7 membrane has the lowest exchange capacity and the highest volume fraction of the intergel spaces filled with an equilibrium electroneutral solution. These properties predetermine the lowest counterion transport number in CJMA-7 among other investigated AEMs, which nevertheless does not fall below 0.87 even in 1.0 eq L⁻¹ solutions of NaCl or Na₂SO₄. One of the reasons for the decrease in the permselectivity of CJMAED membranes is the extended macropores, which are localized at the ion-exchange material/reinforcing cloth boundaries. In relatively concentrated solutions, the electric current prefers to pass through these well-conductive but nonselective macropores rather than the highly selective but low-conductive elements of the gel phase. It is shown that the counterion permselectivity of the CJMA-7 membrane can be significantly improved by coating its surface with a dense homogeneous ion-exchange film.

Keywords: anion exchange membrane; electric conductivity; diffusion permeability; permselectivity; structure-properties relationship; modification

1. Introduction

Over the last 10 years, the number of publications aimed at developing new and improving existing anion exchange membranes (AEMs) has doubled and reached more than 650 articles per year (Scopus). There are several reasons for this interest in AEMs.

The first is the active development of methanol fuel cells [1,2] and redox flow batteries, in particular vanadium flow batteries using AEMs [3]. To ensure high performance of these new devices, AEMs are required that have high hydroxyl ion conductivity, mechanical

robustness and high resistance to aggressive media, in particular, the membranes must be stable in a strongly alkaline environment [4,5].

The second important area is the production of electricity from renewable sources using reverse electro dialysis [6]. Thin, mechanically resistant AEMs with very low electrical resistance are being developed [7] to make this method not only environmentally sound but also economically viable.

The third direction is the use of AEMs in the food and pharmaceutical industries for the demineralization of proteins [8], tartrate stabilization of wine [9], separation of valuable anions of citric, malic, lactic acids and other organic nutrients [10,11]. In this case, the anion-exchange membranes should have sufficiently large pores that do not cause steric hindrances for the transport of large, highly hydrated anions.

The impetus for the activation of the fourth direction was the development of selectrodialysis and metathesis electro dialysis [12,13]. They allow the separation of streams of the ions, the joint presence of which in the concentrate can cause precipitation. Solving this problem revived interest in electro dialysis as an effective method for concentrating reverse osmosis retentates [14], deactivating mine and waste water [11,15], producing high-quality drinking water, water for irrigated agriculture [16], recovery of phosphates from municipal wastewater, livestock liquid effluent and landfills for the production of cheap fertilizers [17] as part of combined baro-electromembrane technologies. AEMs, which are selective to singly charged anions (systems $\text{Cl}^-/\text{SO}_4^{2-}$, for example) [18,19] and are capable of resisting fouling, are essential for this purpose [20].

At the same time, AEMs that were developed and actively used in the 20th century often do not meet these requirements. Their operation in intense current modes, alkaline solutions or solutions of highly hydrated electrolytes leads to the destruction of the ion-exchange matrix [21], inert filler [22] and/or the transformation of strongly basic fixed groups (quaternary amines) into weakly basic tertiary and secondary amines [23]. In addition, the widespread introduction of electro dialysis, dialysis, membrane bioreactors, fuel cells, and other methods has until recently been constrained by the relatively high cost of AEMs.

In order for the new generation of AEMs to meet the above requirements and not have drawbacks, a number of innovations are under development. AEMs with new fixed groups [24], ion-exchange matrices [25], cross-linking agents [26], inert fillers and reinforcing materials [27], as well as methods of membrane manufacturing [28,29] and modifications of their surfaces [6,18,19] are actively developing. These new approaches are summarized in reviews [6,30]. New AEMs of the CJMAED series developed by Hefei Chemjoy Polymer Materials Co. Ltd. (Hefei, China), have a fundamentally different ion-exchange matrix compared to conventional commercial membranes, such as Neosepta AMX (ASTOM Corporation, Japan) and AMH-PES (Mega a.s., Praha, Czech Republic). First of all, they are designed for transport of large, highly hydrated ions and have already shown their effectiveness in extraction of 5'-ribonucleotides from hydrolysate [23], in recovery of gamma-aminobutyric acid (GABA) from reaction mixtures containing salt [31], in purification of methylsulfonylmethane from mixtures containing salt [32], in defluoridation of tea infusion [33], in separation of soluble saccharides from the aqueous solution containing ionic liquids [34] in salt valorization process from high salinity textile wastewater [35], in concentration of the high-salinity solutions prior to being treated by an evaporative crystallizer [36]. At the same time, in some cases, for example, when ED concentrating lithium sulphate from primary resources, new CJMAED membranes demonstrate lower efficiency compared to the traditional Neosepta AMX membrane [37]. Although CJMAED membranes have already found numerous applications, knowledge of their properties is fragmentary. In order to more confidently predict their behavior in new applications, as well as to obtain a fundamental basis for further progress in the synthesis of new membranes, more detailed studies of the structure–property relationship for CJMAED membranes are required.

This work presents the results of a comprehensive study of transport characteristics (electric conductivity, diffusion permeability, transport numbers) of CJMA-3, CJMA-6 and CJMA-7 anion exchange membranes manufactured by the Hefei Chemjoy Polymer Material Co. Ltd. in sodium chloride and sodium sulphate solutions. An analysis of their behavior is carried out in comparison with the widely used Neosepta AMX and AMH-PES membranes. Differences in the structure of these membranes and the impact of these differences on their characteristics are examined. The interplay between the ion exchange capacity, water content, conductivity, diffusion permeability, and counterion transport numbers (counterion permselectivity) of the membranes is studied on the bases of the microheterogeneous model [38]. In addition, we report the results of a surface modification of the CJMA-7 membrane, which significantly improved its counterion permselectivity, that is, decreased undesirable coion transfer. The latter reduces current efficiency of electro dialysis and does not allow obtaining brines of high concentration reducing current efficiency of electro dialysis.

2. Theoretical Background

The microheterogeneous model [38] considers an ion-exchange membrane (IEM) as a two-phase medium (Supplementary materials, Figure S3). One of the phases is the gel phase, which comprises microporous regions consisting of a polymer matrix with fixed groups. The charge of these groups is counterbalanced by a charged solution containing mobile counterions and, to a lesser extent, coions. The filaments of the reinforcing cloth and the inert filler (if any) are also included in the gel phase. The elements of the gel phase are separated by intergel spaces filled with an electrically neutral solution; these are the central parts of the meso- and macropores, together with structural defects of the membrane. It is assumed that there is local equilibrium between the elements of the gel phase and electroneutral solution filling the intergel spaces. When the membrane is in equilibrium with an external solution, the internal electroneutral solution is assumed identical to the external one. This model is used by many researchers to determine the structure–transport properties relationship for IEMs (see, for example [39,40]). The microheterogeneous model gives a simple description of membrane transport characteristics as functions of a single set of parameters, which are the ionic diffusion coefficients (\bar{D}_i) in the gel and solution (D_i) phases, the (dimensionless) volume fractions of the gel phase (f_1) and intergel spaces (f_2 , $f_1 + f_2 = 1$), the Donnan equilibrium constant (K_D), membrane ion-exchange capacity (Q) and a parameter (α), which reflects the relative disposition of the gel and solution phases [38]: $\alpha = -1$ refers to the case where the elements of the gel and solution phases are connected in series; $\alpha = 1$ refers to the case where these elements are connected in parallel. The main equations of the microheterogeneous model are in the Supplementary Materials (SM). The exchange capacities of the membrane and the gel phase (\bar{Q}) are connected by the relation $Q = f_1 \bar{Q}$.

According to the microheterogeneous model [38], within the concentration range $0.1 C_{iso} < C < 10 C_{iso}$ and under condition that parameter α is not too great ($|\alpha| \leq 0.2$), the electrical conductivity of an IEM, κ^* , can be expressed as:

$$\kappa^* = \bar{\kappa} f_1 \kappa f_2 \quad (1)$$

Here C_{iso} is the isoconductance concentration (the concentration at which the conductivities of the membrane, κ^* , gel phase, $\bar{\kappa}$, and bathing solution, κ , are the same); C_{iso} is close to 0.05 eq L^{-1} for conventional IEMs. Here C (eq L^{-1}) is the equivalent electrolyte concentration ($C = |z_1|c_1 = |z_A|c_A$, where subscripts I and A refer to the counterion and coion; c_i (mol L^{-1}) is the molar ion concentration).

In the range of relatively dilute solutions mentioned above, the coion concentration in the gel phase is quite low due to the Donnan exclusion effect. Therefore, the main contribution to the gel phase conductivity is made by the counterions, whose concentration is very close to the concentration of the fixed ions. In these conditions, the value of $\bar{\kappa}$ is

nearly independent of the external concentration, C . Assuming that $\bar{\kappa} = \text{const}$ and κ is proportional to C , we arrive at the following equation connecting κ^* with C :

$$\log \kappa^* \approx f_2 \log C + \text{const} \quad (2)$$

The linearity of the $\log(\kappa^*)$ — $\log(C)$ dependence for conventional IEMs is confirmed in a number of publications [38–40]; the f_2 parameter can be found as the slope of the above dependence. However, this dependence is often determined in a range outside of that close to C_{iso} where Equation (1) holds; parameter α can be rather high (>0.2). In these conditions, the $\log(\kappa^*)$ — $\log(C)$ slope can differ from the true volume fraction of the intergel spaces. Namely, in the range of relatively elevated concentrations, $C > 0.5 \text{ eq L}^{-1}$, the membrane conductivity depends on parameter α . At elevated concentrations, the gel conductivity is much less than the solution conductivity: $\bar{\kappa} \ll \kappa$. When α is small and the series connection of the phases is dominant, the membrane conductivity is controlled by the low-conductive gel regions, and it is relatively small. When α is great and the parallel connection is dominant, the membrane conductivity is high, since it is controlled by the well-conductive intergel solution regions (Figure 1). Therefore, the higher α , the higher the $\log(\kappa^*)$ — $\log(C)$ slope. In any case, the $\log(\kappa^*)$ — $\log(C)$ slope characterizes the contribution of the electroneutral solution filling the intergel spaces into the membrane conductivity. If $C > C_{iso}$, the higher the slope, the higher this contribution. When there is no electroneutral solution in the membrane, the $\log(\kappa^*)$ — $\log(C)$ slope will be minimal, the increase in κ^* is caused only by the coions in the gel phase, where their concentration is very low due to the Donnan exclusion. Maximum slope corresponds to the free solution. Since in the case of near-isoconductance concentration, this slope is equal to f_2 , we call the $\log(\kappa^*)$ — $\log(C)$ slope the apparent fraction of the electroneutral solution in the membrane, $f_{2app} = d \log \kappa^* / d \log C$.

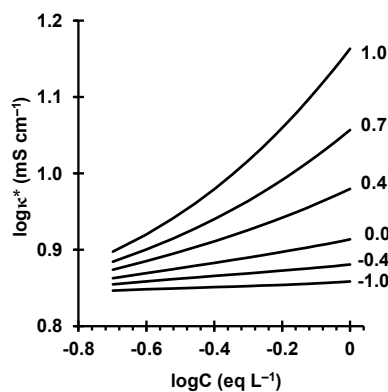


Figure 1. $\log \kappa^*$ — $\log C$ dependence at a fixed volume fraction of intergel solution, f_2 , and different α (shown near the curves) calculated according to the microheterogeneous model [38] for the membrane parameters related to the AMH-PES membrane.

At $C = C_{iso}$, the conductivity of the gel phase, $\bar{\kappa}$, can be approximately (when neglecting the contribution of the coions, which is generally insignificant) presented as follows:

$$\bar{\kappa} = \frac{z_1 \bar{D}_1 \bar{Q} F^2}{RT}, \quad (3)$$

$$\bar{Q} = \frac{Q}{f_1}, \quad (4)$$

where \bar{Q} is the concentration of the fixed ions in the gel phase; z_1 is the counterion charge number, subscript 1 refers to the counterion; F , R , and T are the Faraday constant, absolute temperature, and gas constant, respectively.

The differential (or local) diffusion permeability coefficient, P^* , is defined from the transport equation deduced within the irreversible thermodynamics [38,41]:

$$j_i = -P^* \frac{dc_i}{dx} + \frac{it_i^*}{z_i F} \quad (5)$$

where i is the current density, j_i and t_i^* are the flux density and the transport number of ion i in the membrane, c_i is the molar concentration of this ion in the "virtual" (or "corresponding" [41]) solution, which is an electrically neutral solution being in equilibrium with a thin membrane layer with coordinate x . The asterisk means that the quantity refers to a small membrane volume with coordinate x .

The differential and integral permeability coefficients are linked as follows [38]:

$$P^* = P + C \frac{dP}{dC} \quad (6)$$

Equation (6) can be presented in the form [42]:

$$P^* = P(1 + \beta), \quad (7)$$

where $\beta = d \log P / d \log C$. Equation (7) is obtained from Equation (6) as follows: $P + C \frac{dP}{dC} = P \left(1 + \frac{C}{P} \frac{dP}{dC} \right) = P \left(1 + \frac{d \log P}{d \log C} \right) = P(1 + \beta)$.

The value of P^* can be found from the concentration dependence of P presented in bilogarithmic plot ($\log P$ vs. $\log C$). The slope of this dependence gives β .

If the external solution concentration is not too high, an approximate form of the Donnan relation can be used to calculate the coion concentration in the gel phase: $\bar{c}_A = K_D c_A^2 / \bar{Q}$ (written for a 1:1 electrolyte [38]). Using the last relation, an approximate formula to calculate P^* in nonconcentrated solutions (up to 1 mol L⁻¹) can be obtained:

$$P^* = 2D_A t_1^* \left[f_1 \left(K_D \frac{\bar{D}_A c_A}{D_A \bar{Q}} \right)^\alpha + f_2 \right]^{1/\alpha} \quad (8)$$

Thus, the membrane diffusion permeability is controlled by the coion diffusion in the gel phase and in the intergel spaces. The former is determined by the parameter $G = K_D \bar{D}_A / \bar{Q} D_A$, first proposed by Gnusin [43]. This parameter reflects both the ability of the gel phase to coion sorption (the K_D / \bar{Q} ratio) and the coion mobility in this phase (the \bar{D}_A / D_A ratio). The electrolyte diffusion through the intergel solution is controlled by the f_1 (f_2) and α parameters, as well as by D_A . When applying parameter G , only four parameters are needed to describe the transport properties of IEMs: \bar{Q} , G , f_1 (f_2), and α . To find them by fitting the experimental concentration dependencies of κ^* and P^* , we use the feature that f_2 mainly determines the slope of the $\log(\kappa^*)$ — $\log(C)$ curve, while \bar{Q} shifts the curve up or down; a similar role is played by α and G when treating $\log(P^*)$ — $\log(C)$ curve.

The values of κ^* and P^* allow determination of the transport numbers of counterions (t_1^*) and coions (t_A^*) in an IEM according to an approximate relation [44]:

$$t_1^* = \frac{1}{2} + \sqrt{\frac{1}{4} - \frac{(z_1 |z_A|) P^* F^2 C}{(z_1 + |z_A|) R T \kappa^*}}, \quad t_A^* = 1 - t_1^* \quad (9)$$

3. Membranes

3.1. Manufacturing

Conventionally, ion-exchange membranes are classified as homogeneous and heterogeneous. Heterogeneous membranes (which historically were produced earlier) are prepared by using powdered ion-exchange resin, which is mixed with a powder of a filler, such as polyethylene. The ion-exchange material (the particles of ion-exchange resin) is unevenly and sometimes discontinuously distributed in the membrane. Homogenous membranes

are prepared by introducing an ion-exchange moiety directly into the structure of the constitutive polymer [45]. In this case, the ion-exchange material forms a continuous phase, which is relatively evenly distributed in the membrane. The reinforcing cloth (tissue, fabric) is added to both homogeneous and heterogeneous membranes. There are a few types of membranes (such as some marques of Nafion), which do not contain reinforcing cloth.

The commercial CJMA-3, CJMA-7 [46] and experimental CJMA-6 homogeneous AEMs are manufactured by the Hefei Chemjoy Polymer Materials Co. Ltd. (Hefei, China). The generic name of this type of membrane CJMAED on the manufacturer's website emphasizes their possible use in electrodialysis. Their ion-exchange matrix contains polyvinylidene fluoride, PVDF (CJMA-3), or polyolefin (CJMA-6, CJMA-7) functionalized with quaternary ammonium groups [31]. The matrix is crosslinked through the side chains [47]. These membranes are produced by the casting method and are reinforced with polyethylene terephthalate, PET (trademarks: Terylene, or Lavsan, or Dacron) cloth by hot rolling. The CJMAED membranes differ from each other in the type of polymer matrix, in the degree of crosslinking and in the concentration of fixed groups. These membranes are less costly compared with other anion-exchange membranes on the world market.

The Neosepta AMX (ASTOM Corporation, Tokyo, Japan) and Ralex AMH-PES (Mega a.s., Czech Republic) anion exchange membranes have a highly crosslinked aromatic ion exchange matrix based on copolymer of polystyrene (PS) and divinylbenzene (DVB). These membranes also mainly contain quaternary ammonium groups. The pseudohomogeneous Neosepta AMX membrane is produced using the "paste method" [48]. The reinforcing PVC cloth as well as PVC particles with diameter less than 60 nm (inert filler) are introduced into the membrane at the stage of the ion-exchange matrix polymerization [49]. The AMH-PES heterogeneous membrane is produced by hot rolling of the mixture of a fine powder of the ion-exchange resin Lewatit M500 with an average diameter of about 5 microns and low density polyethylene (PE), at an approximate ratio of 2:1 [50]. A reinforcing Ulester 32S net is rolled into both sides of the AHM-PES membrane while the membrane is still hot [51,52]. The data on the membranes under study are summarized in Table 1.

Table 1. Materials and methods of manufacturing the membranes under study.

Membranes	Fixed Groups	Ion-Exchange Matrix	Inert Filler	Methods of Manufacturing	Reinforcing Cloth	Method of Embedding Reinforcing Cloth
AMX	Mainly $-N^+(CH_3)_3$	DVB/PS	PVC	"Paste method"	PVC	Casting the paste on the cloth
AMH-PES			PE	Hot rolling	Ulester 32S	Hot rolling
CJMA-3		PVDF	Absent	Casting	PET	Casting the paste on the cloth
CJMA-6 CJMA-7		Polyolefin				

3.2. Surface and Cross-Section Visualization

Figures 2 and 3 demonstrate optical images of the surfaces and cross-sections of swollen AEMs. The obtained AMX and AMH-PES images are in good agreement with the known results of numerous studies of their structure, presented, for example, in [52–54]. Reinforcement cloth is evenly distributed over the cross-section of the AMX membrane (Figure 2a). Both surfaces of this membrane are wavy. The characteristic distance between the "peaks" and "valleys" of the AMX surface relief is determined by the periods of undulation of the filaments of reinforcing cloth and is 250 μm . The difference between the highest and lowest points of the waves is $15 \pm 5 \mu\text{m}$. The AMX membrane has practically no macropores [55] due to the good adhesion between the PVC reinforcing cloth and the ion exchange composite, which contains PVC as an inert filler.

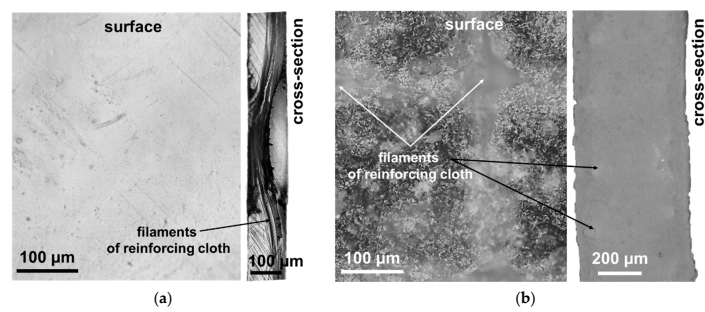


Figure 2. Optical images of surfaces and cross-sections of AMX (a), AMX-PES (b) membranes.

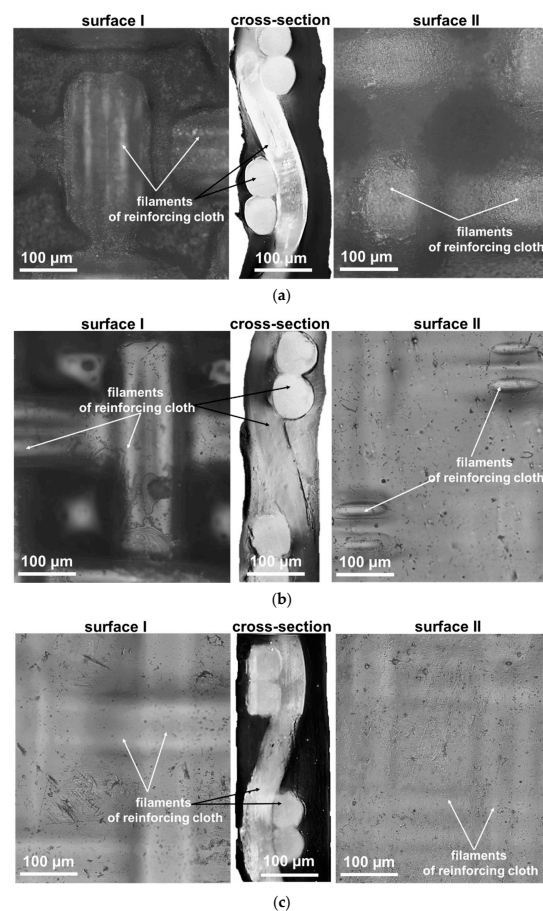


Figure 3. Optical images of surfaces and cross-sections of CJMA-3 (a), CJMA-6 (b) and CJMA-7 (c) membranes.

Reinforcing cloth is located near both surfaces of the heterogeneous AMH-PES membrane (Figure 2b) and the threads sometimes jutted from the ion-exchange material [51]. These protrusions, as well as those of the ion exchange resin particles, are responsible for the surface roughness of the AMH-PES. The difference between the highest and lowest points of the AMH-PES surface is $15 \pm 2 \mu\text{m}$. Macropores are mainly localized at the ‘ion exchange resin/PE’ and ‘reinforcing cloth/composite ion exchange material’ boundaries [56]. The reinforcing cloth of all CJMAED membranes is localized closer to one of the surfaces (surface I). As a result, surface II is smoother and surface I is wavier (Figure 3). Moreover, the bulges are localized over the intersections of the threads of the reinforcing cloth. In these places the filaments sometimes protrude above the ion-exchange material. The distance between two neighboring highest points of the surface is determined by the cell step of the reinforcing cloth, equal to $250 \mu\text{m}$. Spread of heights of the surface I can reach $80 \mu\text{m}$ that significantly exceeds the undulation of the AMX surface. The difference in the geometric

characteristics of surfaces I and II for the studied CJMAED membranes increases with increasing membrane thickness in the sequence: CJMA-6 < CJMA-3 < CJMA-7. Note that the optical images of the swollen CJMA-3 membrane surfaces are in good agreement with its SEM images obtained for dry samples [56].

Extended macropores are localized at the boundaries between the filaments of reinforcing cloth and the ion-exchange material of CJMAED membranes. These macropores are visualized as light stripes in images of the swollen sample exposed to air with surface I (Figure 4). They appear at the crosshairs of the reinforcing filaments that are closest to the surface during the first few seconds of drying of the test sample. As it dries, these light stripes spread along the entire length of the reinforcing filaments. As will be shown in Section 5, the presence of such macropores, that are in contact with the external solution due to the protrusions of the reinforcing cloth filaments to the surface, can strongly affect the transport characteristics of CJMAED membranes.

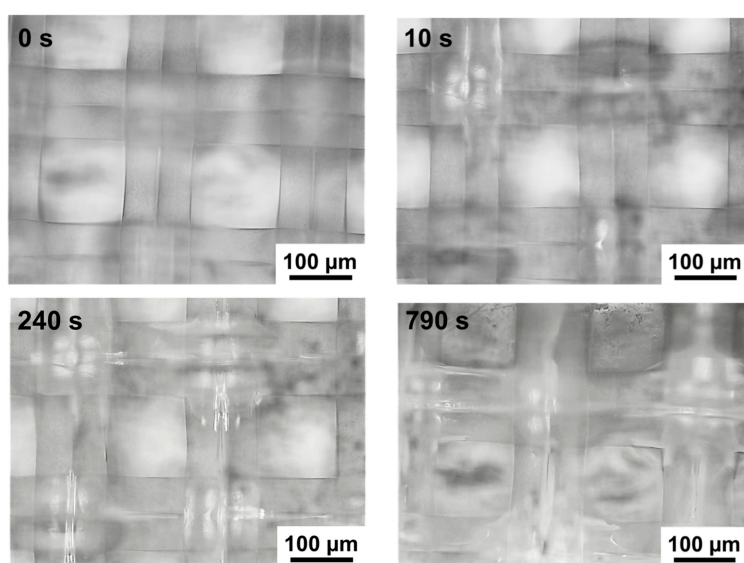


Figure 4. Optic visualization of the swollen CJMA-7 membrane drying process. The time of contact of the surface I with air in seconds is indicated on each video frame.

4. Membranes Characterization

4.1. Basic Characteristics

Table 2 summarizes some of the characteristics of the studied AEMs that we obtained or found in the literature.

The thickness of the swollen heterogeneous AMH-PES membrane is several times greater than that of the swollen homogeneous membranes, which increase in the following order: CJMA-6 < AMX < CJMA-3 < CJMA-7. The exchange capacities of swollen membranes (Q) having an aromatic matrix (AMX, AMH-PES) significantly exceed the values found for CJMAED membranes, for which Q increases in the series: CJMA-3 < CJMA-7 < CJMA-6. Concentration of fixed groups (the number of millimoles of fixed groups per 1 cm³ of water in the membrane), C_X , grows in the following order: CJMA-7 << CJMA-3 \approx AMH-PES < CJMA-6 < AMX. The difference in the sequences found for C_X and Q is caused by a twofold increase in the water content in the AMH-PES and CJMA-7 membranes compared to the other membranes under study. As expected, the density of the highly hydrated AMH-PES and CJMA-7 membranes approaches that of water. The density of the less hydrated AMX, CJMA-3 and CJMA-6 membranes is more dependent on the density of the polymers [57] from which they are made. The thickest AMH-PES membrane has the highest electrical resistance in a moderately concentrated (0.5 M) NaCl solution. In the next section, we will try to explain the order in which the electrical resistance of homogeneous membranes increases: CJMA-7 < AMX \approx CJMA-3 < CJMA-6.

Table 2. Some characteristics of the studied membranes. Our data are in bold without references.

Membranes	Thickness of AEM in 0.02 M NaCl, μm	Ion-Exchange Capacity of Swollen AEM, $\text{mmol/g}_{\text{wet}}$	Water Content, $\text{gH}_2\text{O/g}_{\text{dry}}$, %	Concentration of Fixed Groups in Swollen AEM, $\text{mmol cm}^{-3} \text{H}_2\text{O}$ ²	Water Content, $\text{mol H}_2\text{O/mol Fixed}$ Groups	Density of Swollen AEM, g cm^{-3}	Resistance of AEM in 0.5 M NaCl Solution, Ohm cm^2
DVB/PS ion exchange matrix							
AMX	135 ± 5 141 ± 6 [58]	1.25 ± 0.05 1.25 [59]	19 ± 1 10–14 [60] 34 [61]	7.7 ± 1.0	7.2 ± 1 6.1 [58] 7.8 [62]	1.22 ± 0.05 1.10 [60]	2.9 ± 0.5 2.7 [63] 2.15 [61]
AMH-PES	543 ± 10 550 ± 3 [52]	1.33 ± 0.01 1.25 ± 0.08 [52] 0.86 [64]	46 ± 5 56 [65] 45.2 [64]	4.2 ± 1.0	13.3 ± 0.7 17.8 ± 1.0 [52]	1.06 ± 0.05 1.12 [66]	6.4 ± 0.5 6.1 [64] <7.5 [67] 7.66 [65]
PVDF or Polyolefin ion exchange matrix							
CJMA-3	151 ± 5 150 ± 20 ¹ 130 [68] 250 [31]	0.57 ± 0.05 0.5–0.6 ¹ 0.9 [68] 1.45 [31]	17 ± 1 15–20 ¹ 26 [69] 35–45 [31]	4.0 ± 1.0	14.0 ± 1.0	1.39 ± 0.05	5.1 ± 0.5 4.0 ± 0.5 ¹ 2 [68] 3–6 [31]
CJMA-6	120 ± 3 130 ± 10 [36]	0.90 ± 0.05 0.5–0.7 ¹	18 ± 1 35–37 [36]	6.0 ± 1.0	9.2 ± 1.0	1.32 ± 0.05	2.9 ± 0.5 2.5–3.0 [53]
CJMA-7	174 ± 10 150 ± 20 ¹ 200 [70]	0.75 ± 0.05 0.9–1.0 ¹ 0.8 ± 1.0 [70]	39 ± 2 28–30 ¹ 35–40 [70]	2.6 ± 1.0	21.7 ± 1.0	1.13 ± 0.05	1.4 ± 0.5 1.5 ± 1.8 ¹ 1.5–2.5 [70]

¹ The data were provided by the manufacturer [46]. ² The number of millimoles of fixed groups per 1 cm³ of water in the membrane.

4.2. Transport Properties

4.2.1. Electrical Conductivity

As already mentioned in Section 2, Equation (2), which was obtained in the framework of the microheterogeneous model, is fulfilled in the concentration range $0.1C_{iso} < C < 10C_{iso}$, where C_{iso} is the concentration isoelectric conductivity. From Equations (2) and (3) it follows: near C_{iso} , the electrical conductivity of the membrane in the first approximation is determined by the exchange capacity of the gel phase (the concentration of fixed groups \bar{Q}) and the mobility of counterions in this phase, equal to $z_1\bar{D}_1F/RT$. Note that the higher the water content of the membrane per fixed group, the higher the mobility. The higher \bar{Q} , the higher the electrical conductivity of the gel phase, $\bar{\kappa}$, and, accordingly, that of the membrane, κ^* . With an increase in C , the value of $\bar{\kappa}$ changes insignificantly, mainly due to the sorption of coions. At the same time, the conductivity κ of the intergel space (the central part of the pores) filled with a solution identical to the external one increases nearly proportional to C . With increasing C , the effect of the values of κ , f_{2app} , and α on the membrane electrical conductivity rises. As mentioned above, the value of f_{2app} increases with increasing concentration. It is due to increasing contribution of the intergel solution to the overall membrane conductivity; in addition, in the range of elevated concentrations, coions are more and more involved in the conductivity of the gel phase because of their increasing sorption by the gel. The properties of membranes differ most of all in the region of high concentrations. For these reasons, the f_{2app} values were determined in the 0.4–1.0 eq L⁻¹ concentration range, where 1.0 eq L⁻¹ is the maximum concentration used in the study.

Figure 5 shows concentration dependencies of the conductivity of AEMs in NaCl and Na₂SO₄ solutions. Table 3 summarizes the values of the membrane parameters found from these dependencies along with the data on the membrane diffusion permeability measured as the functions of concentration (Section 4.2.2). These parameters are the input parameters for the microheterogeneous model [38]. The values of these parameters were found by fitting the results of modelling to the experimental data. We have used the following features of the model behavior: when fitting the κ^* vs. C dependence, the f_2 value controls the slope of the $\log\kappa^*$ vs. $\log C$ curve, while \bar{D}_{Cl-} shifts the curve up (when \bar{D}_{Cl-} increases) or down (when it decreases); when fitting the P^* vs. C dependence, similarly, the slope and position of the $\log P^*$ vs. $\log C$ may be changed by varying the values of parameters α and $G = K_D\bar{D}_{Na^+}/(\bar{Q}D_{Na^+})$. Generally, there is a good agreement with the data known in the literature. As Figure 5 shows, the difference between the calculated and experimental results does not exceed the experimental error.

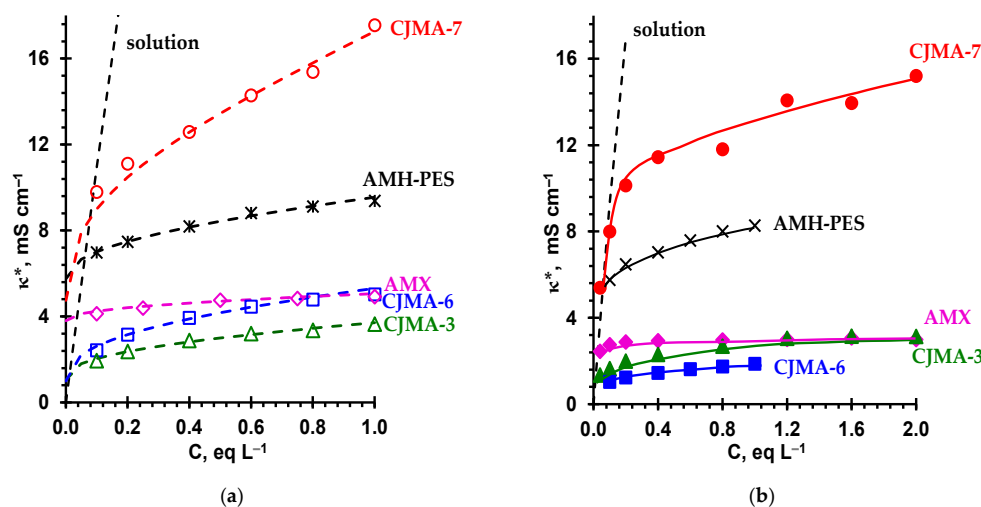


Figure 5. Concentration dependencies of the AEMs' conductivity in NaCl (a) and Na₂SO₄ (b) solutions. Markers are experimental data; dashed lines are calculations using the microheterogeneous model [38]. The solid lines in (b) are drawn to guide the eye.

Table 3. Parameters of the microheterogeneous model for AEMs (found for the case of NaCl bathing solutions): the Cl^- counterion diffusion coefficient (\bar{D}_{Cl^-}) in the gel phase, ion-exchange capacity (\bar{Q}) of this phase, Gnuisn's parameter (G), structural parameter (α), apparent (f_{2app}) and "true" (f_2) volume fractions of the intergel solution of swollen membranes in NaCl and Na_2SO_4 solutions, as well as and the ratio of the SO_4^{2-} to Cl^- diffusion coefficients in the gel phase. The value of f_{2app} is found in the concentration range from 0.4 to 1.0 eq L^{-1} .

Membranes	$\bar{D}_{\text{Cl}^-} \times 10^6$ $\text{cm}^2 \text{s}^{-1}$	$\frac{\bar{D}_{\text{SO}_4^{2-}}}{\bar{D}_{\text{Cl}^-}}$	f_{2app}		f_2	\bar{Q} , mmol cm^{-3}	$G \times 10^3$ $\text{mmol}^{-1} \text{cm}^3$	α
			NaCl	Na_2SO_4	NaCl			
AMX	0.70	0.3 ± 0.2	0.10 ± 0.02 0.11 [40] 0.099 [60]	0.11 ± 0.02	0.03 ± 0.02	1.5 ± 0.1 1.39 [60]	0.32	0.39 ± 0.04
AMH-PES	1.20	0.4 ± 0.2	0.15 ± 0.02 0.14 [52]	0.17 ± 0.02	0.06 ± 0.02	1.5 ± 0.1 1.5 [52]	1.40	0.41 ± 0.04
CJMA-3	0.43	0.4 ± 0.2	0.27 ± 0.02	0.27 ± 0.02	0.12 ± 0.02	0.9 ± 0.1	0.17	0.28 ± 0.04
CJMA-6	0.32	0.7 ± 0.2	0.30 ± 0.02	0.29 ± 0.02	0.17 ± 0.02	1.4 ± 0.1		0.23 ± 0.04
CJMA-7	2.30	0.6 ± 0.2	0.35 ± 0.02	0.39 ± 0.02	0.18 ± 0.02	1.0 ± 0.1	8.4 ± 3	0.30 ± 0.04

The AMH-PES membrane is a heterogeneous one, hence it contains macropores. In addition, this membrane is relatively highly hydrated (Table 2), which leads to a higher ion mobility in the gel phase and a lower effect of Donnan coion exclusion (Table 3). As a result, the values of \bar{D}_{Cl^-} and G for this membrane are elevated, and the f_{2app} value is about 1.5 times greater than that for the homogeneous AMX membrane. In the studied concentration range ($C > C_{iso}$) of NaCl solutions, the conductivity of AMH-PES is significantly higher than the AMX conductivity (Figure 5a). Moreover, in accordance with the microheterogeneous model, this difference increases with increasing concentration of the external solution.

The CJMAED membranes have elevated values of f_{2app} . At concentrations of the external solution close to C_{iso} , the conductivity, according to Equation (3), is determined by the product of \bar{Q} and \bar{D}_{Cl^-} . The latter mainly depends on the water uptake by the gel phase, the maximum is for the CJMA-7 membrane, accordingly, the counterion mobility in the gel phase of this membrane is the greatest one among the studied membranes. The \bar{D}_{Cl^-} values are not very different for the CJMA-3 and CJMA-6 membrane, but \bar{Q} is higher for the latter, which determines its higher conductivity compared to the CJMA-3 membrane. With an increase in the concentration of the external solution, the conductivity of CJMA-6 grows faster than the conductivity of CJMA-3, but the difference between them remains small. At the same time, the difference between the conductivities of CJMA-6 and AMH-PES membranes decreases with increasing concentration due to the fact that the f_{2app} value for CJMA-6 is about two times higher than that for AMH-PES. The highest values of conductivity (and the lowest values of electrical resistance, Table 2) in the studied range of NaCl concentrations are demonstrated by the CJMA-7 membrane, for which the f_{2app} parameter is about 0.35. Note that f_{2app} for this membrane is significantly higher than that for the heterogeneous MK-40 and MA-41 membranes ($f_{2app} = 0.21 \pm 0.03$) [71]. This experimental fact allows us to conclude that the CJMA-7 membrane contains an ion-exchange material, which has more large pores in comparison with other membranes under study. The dimensions of the pores in the ion-exchange materials of the CJMA-3 and CJMA-6 membranes are apparently significantly smaller.

Replacing the singly charged Cl^- counterion with the doubly charged SO_4^{2-} counterion results in a decrease in the conductivity of all studied AEMs (Figure 5b). Estimates made using the microheterogeneous model [38] allow us to conclude that in the gel phase of AMX, AMH-PES and CJMA-3 membranes, the ratio of diffusion coefficients of doubly charged and singly charged counterions is 0.3–0.4 (Table 3), while in solution at infinite dilution (Table S1, Supplementary Materials) $D_{\text{SO}_4^{2-}}/D_{\text{Cl}^-} = 0.5$. In the literature, such a decrease is explained by lower mobility of doubly charged counterions as a result of ion–ion interactions simultaneously with two fixed groups [72,73] and/or steric hindrances

caused by the large size of strongly hydrated ions [74,75], which are sulfate ions (Table S1, Supplementary Materials). Low values of the conductivity of the Na_2SO_4 solution in the intergel spaces also contributes to the lower values of the conductivity of the membranes in this solution.

In the case of CJMA-6 and CJMA-7 membranes, which are characterized by the highest f_{2app} values, the ratio $\overline{D}_{\text{SO}_4^{2-}}/\overline{D}_{\text{Cl}^-}$ increases. This means that the structural features of the ion-exchange matrix of these membranes make it possible to at least partially remove the restrictions on the transport of sulfate ions in comparison with chloride ions. This property of the new CJMA-6 and CJMA-7 membranes is very attractive for their use in the electro dialysis processing of sulfate and other solutions containing large anions.

4.2.2. Diffusion Permeability

The concentration dependences of the integral coefficient of diffusion permeability, P , for the studied AEMs, as well as the counterion transport numbers in these membranes are shown in Figures 6 and 7, respectively.

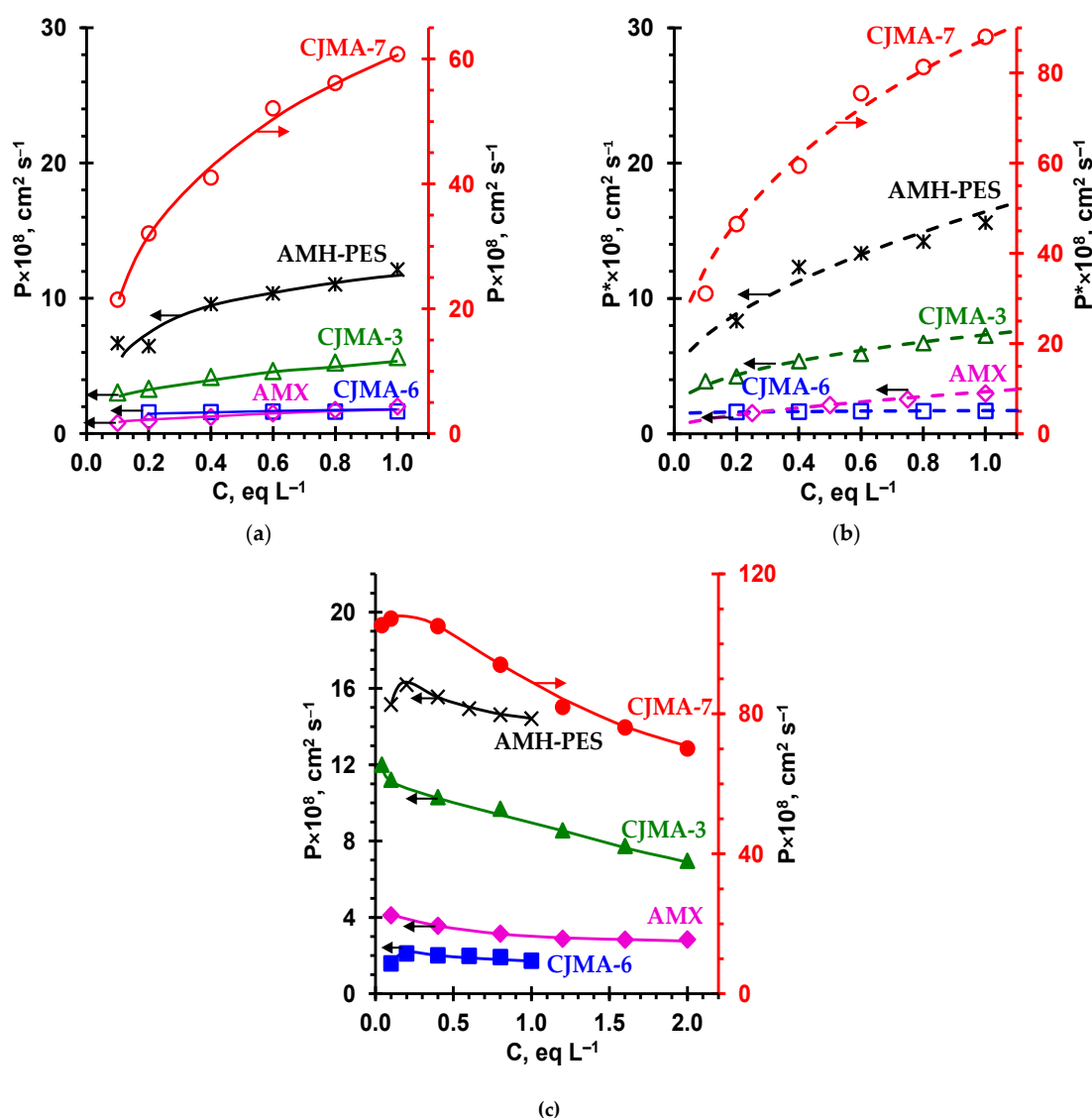


Figure 6. Concentration dependencies of the integral coefficient of diffusion permeability of AEMs in NaCl (a) and Na_2SO_4 (c) solutions as well as concentration dependency of the differential coefficient of diffusion permeability of AEMs in NaCl (b). Markers are experimental data; dashed lines are calculations using the microheterogeneous model [38]. The solid lines in (a) and (c) are drawn to guide the eye.

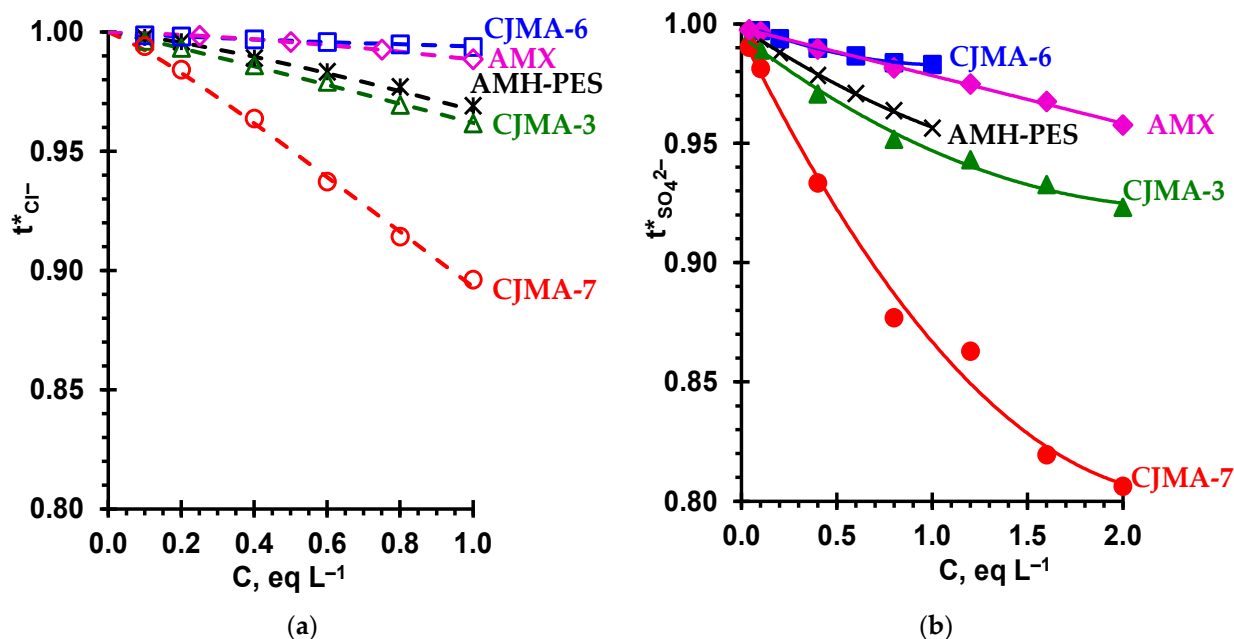


Figure 7. Concentration dependencies of counterion transport numbers in the AEM under study in NaCl (a) and Na₂SO₄ (b) solutions. The dashed lines in (a) are calculations using the microheterogeneous model [38]. The solid lines in (b) are drawn to guide the eye.

In the case of the CJMA-7 membrane, the values of P in NaCl solution are several times higher than the corresponding value for the AMH-PES membrane and are more than one order of magnitude higher than the P for the AMX, CJMA-6 and CJMA-3 membranes. Apparently, the dominant role is played by the diffusion of electrolyte through the macropores of the CJMA-7 membrane. Three parameters contribute to the diffusion permeability according to the microheterogeneous model [38]: \bar{Q} , f_1 (f_2) and α .

The influence of these parameters on the differential diffusion coefficient of AEMs, P^* (see the definition of P^* in Section 2), can be expressed by the following equation [55]:

$$P^* = \left\{ \left[f_1 \left(\frac{\bar{P}}{t_1} \right)^\alpha + f_2 \left(\frac{D}{t_1} \right)^\alpha \right]^{-1/\alpha} + \left[f_1 \left(\frac{\bar{P}}{t_A} \right)^\alpha + f_2 \left(\frac{D}{t_A} \right)^\alpha \right]^{-1/\alpha} \right\}^{-1}, \quad (10)$$

where \bar{t}_1 and t_1 , as well as \bar{t}_A and t_A are the counterion and coion transport numbers in the gel phase and solution, respectively. The diffusion permeability of the gel phase for 1:1 electrolyte (NaCl) and 2:1 electrolyte (Na₂SO₄) can be approximated as [55]:

$$\bar{P} = 2\bar{t}_1\bar{D}_A K_D \left(\frac{C}{\bar{Q}} \right), \quad |z_1| = |z_A| = 1 \quad (11)$$

$$\bar{P} = \frac{3}{2}\bar{t}_1\bar{D}_A K_D \left(\frac{C}{\bar{Q}} \right)^{1/2}, \quad |z_1| = 2, |z_A| = 1 \quad (12)$$

where C is the equivalent concentration of external solution ($C = z_i c_i$).

The AMX and AMH-PES membranes have close values of \bar{Q} (Table 3) and similar ion exchange matrices based on DVB/PS (Tables 1 and 3). The similarity of the matrices predetermines close values of α (Table 3). Therefore, as predicted by the model, the diffusion permeability of these membranes increases with growth of external solution NaCl concentration in order AMX < AMH-PES according to the increase in the volume fraction f_2 of the intergel solution. The CJMA-6 and CJMA-7 membranes have close values of f_2 , but different values of \bar{Q} . According to Equations (11) and (12), \bar{P} is inversely proportional

to \bar{Q} : the higher the concentration of fixed groups, the stronger the Donnan exclusion of coions from the gel phase [72]. A very low permeability of the gel phase of the CJMA-6 membrane is characterized by an extremely small value of parameter G (Table 3).

The value of α plays also an important role, which influences the slope of $\log(P^*) - \log(C)$ curve: the greater α , the greater the value of P^* (but the lower the slope). The highest rate of diffusion can be obtained when $\alpha = 1$ and the electrolyte freely passes across the through pores. With decreasing α , the electrolyte needs to overcome more and more of the gel phase elements, which are significant barriers to coions. Among the three CJMAED membranes, the CJMA-7 membrane has the highest values of α ; as well, the values of f_2 and f_{2app} are the highest for this membrane. In addition, the value of G , which characterizes the ability of coions to cross the gel phase, is especially great. As a result, the value of P^* for this membrane is only 25 times lower than the NaCl diffusion coefficient in solution. For the CJMA-3 membrane this factor is about 250, and for the CJMA-6 and AMX membranes it is equal to 750 (all values are given for the case of 1 eq L⁻¹ NaCl solution). The importance of parameters α and G also follows from the fact that the value of P^* for the CJMA-6 membrane is significantly lower than for the AMX, despite the higher f_2 (CJMA-6) and the close \bar{Q} (Table 3).

The replacement of a NaCl solution with a Na₂SO₄ solution with the same normality leads to a noticeable increase in the diffusion permeability of all studied membranes (Figure 3). A similar trend was found for a Russian heterogeneous anion-exchange MA-41 membrane earlier [76]. From Equations (11) and (12) it follows that $\bar{P}_{NaCl} < \bar{P}_{Na_2SO_4}$, if we take into account that the value $C/\bar{Q} < (C/\bar{Q})^{1/2}$, when C/\bar{Q} is significantly less than unity. The increase in the diffusion permeability of the gel phase is caused by an increase in the coion concentration in this phase due to increasing electrostatic interactions between counterions and coions. Another reason for the increase in the diffusion permeability of membranes in Na₂SO₄ solutions can be a slight increase in f_2 (f_{2app}) (Table 3). The latter is caused by the stretching of the ion-exchange matrix [72] when highly hydrated sulfate ions (Table S1, Supplementary Materials) are introduced into its pores. A similar effect, confirmed by the data of standard contact porosimetry, was observed in our study of the diffusion permeability of AEMs in phosphate-containing solutions [55].

It follows also from Equations (11) and (12) that the value of \bar{P} should increase with increasing concentration of the external solution. Indeed, the diffusion permeability of AEMs increases with increasing NaCl solution concentration (Figure 6a,b). At the same time, a slight increase in the diffusion permeability of AEMs in dilute Na₂SO₄ solutions is replaced by a decrease when increasing the Na₂SO₄ concentration (Figure 6c). This, at first glance, an unexpected feature in the shape of the P vs. C dependence, apparently, is caused by a sharp drop in the diffusion coefficient of Na₂SO₄ (D) with an increase in the solution concentration (Figure S1, Supplementary Materials).

The transport numbers of the Cl⁻ (Figure 7a) and SO₄²⁻ counterions (Figure 7b), which characterize the selectivity of AEMs with respect to anion transport, decrease in a series that, according to Equation (9), corresponds to an increase in the P^*/κ^* ratio. Higher diffusion permeability of membranes in Na₂SO₄ solutions and their lower conductivity in the SO₄²⁻-form result in lower values of $t_{SO_4^{2-}}^*$ compared to $t_{Cl^-}^*$.

The AMX and CJMA-6 membranes demonstrate the highest and nearly the same counterion permselectivity in the investigated range of electrolyte concentrations. The selectivity of the AMH-PES and CJMA-3 membranes is noticeably lower, as mentioned above, due to either the higher values of f_{2app} and α (AMH-PES), or the low exchange capacity (CJMA-3). The CJMA-7 membrane has the lowest selectivity, since it is characterized by the highest f_{2app} and a sufficiently large α . Note that in moderately dilute (0.1 eq L⁻¹) NaCl and Na₂SO₄ solutions, the t_1^* value for all membranes, except for CJMA-7, is close to unity. Moreover, even in concentrated (1.0 eq L⁻¹) NaCl and Na₂SO₄ solutions, the t_1^* values for these membranes (except for CJMA-7) exceed 0.95. This means that these membranes can be used in electrodialysis for both demineralization and concentration of solutions.

Below we show that the selectivity of the CJMA-7 and similar membranes with a high f_{2app} value can be improved by at least partially eliminating structural defects caused by the embedding of the reinforcing cloth (see Section 3.2).

5. Increasing CJMA-7 Permselectivity by Surface Modification

Optical images (Figure 3) allow us to see some filaments of CJMA-7 reinforcing cloth protruding to the surface. This causes formation of large macropores whose mouths open into the external solution. These large and long pores facilitate the access of the external solution into the membrane bulk. We assume that this defect is one of the main reasons for the low permselectivity of the CJMA-7 membrane. We try to reduce this defect by covering the membrane surface with a dense ion-exchange film. For this purpose, we used a sample designated as CJMA-7', which is the CJMA-7 membrane that was stored in a refrigerator at a temperature of +8 °C in a 0.1 N NaCl solution for 10 months.

A 4 µm thick film of sulfonated fluoropolymer MF-4SK was then formed on the surface of the CJMA-7' sample. The CJMA-7'M-25 and CJMA-7'M-50 samples were obtained according to the procedure described in Section 6.2. A sample of the CJMA-7' membrane, which was used for comparison, was in the air for the same time (24 h) and at the same temperature (+25 °C) as the sample CJMA-7'M-25 during its preparation. Sample CJMA-7'M-50 was kept at 50 °C for the last 1 h of modification. Figure 8 shows the scheme of the treatment applied to the CJMA-7 membrane.

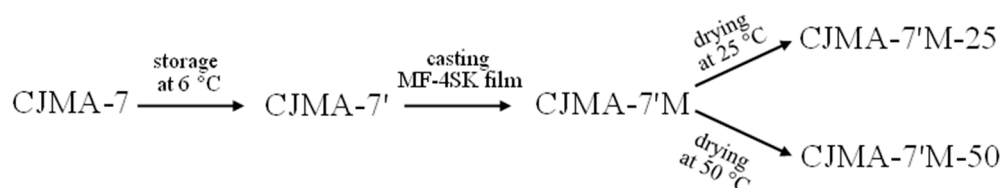


Figure 8. Scheme of the treatment applied to the CJMA-7 membrane.

Figure 9 shows the concentration dependences of the conductivity of the pristine membrane and modified samples. Figure 10 shows the diffusion permeability and coion transport numbers (t_A^*) in the original membrane and modified samples. The data were obtained in NaCl solutions.

A prolonged exposure of the CJMA-7 membrane at a relatively low (8 °C) temperature for a long time resulted in a slight decrease in electrical conductivity (Figure 9b), as well as in an almost twofold decrease in the diffusion permeability (Figure 10a) and more than twofold decrease in the coion transport number (Figure 10b) compared to the pristine membrane. These changes are apparently caused by the contraction of the weakly cross-linked ion exchange matrix during storage of this membrane. It is known, for example, that in the case of Nafion materials, the relaxation of their aliphatic matrix after exposure to temperature takes 1000 or more hours [77]. From the data presented in Figures 9 and 10 it can be seen that the application of a film on the CJMA-7' membrane results in a more significant reduction (by about 60%) in the conductivity. At the same time, the diffusion permeability of CJMA-7' decreased even more significantly, which led to a noticeable decrease in the coion transport numbers: by 10% in the case of drying at 25 °C (the CJMA-7'M-25 membrane) and by 40% in case of drying at 50 °C (the CJMA-7'M-50 membrane).

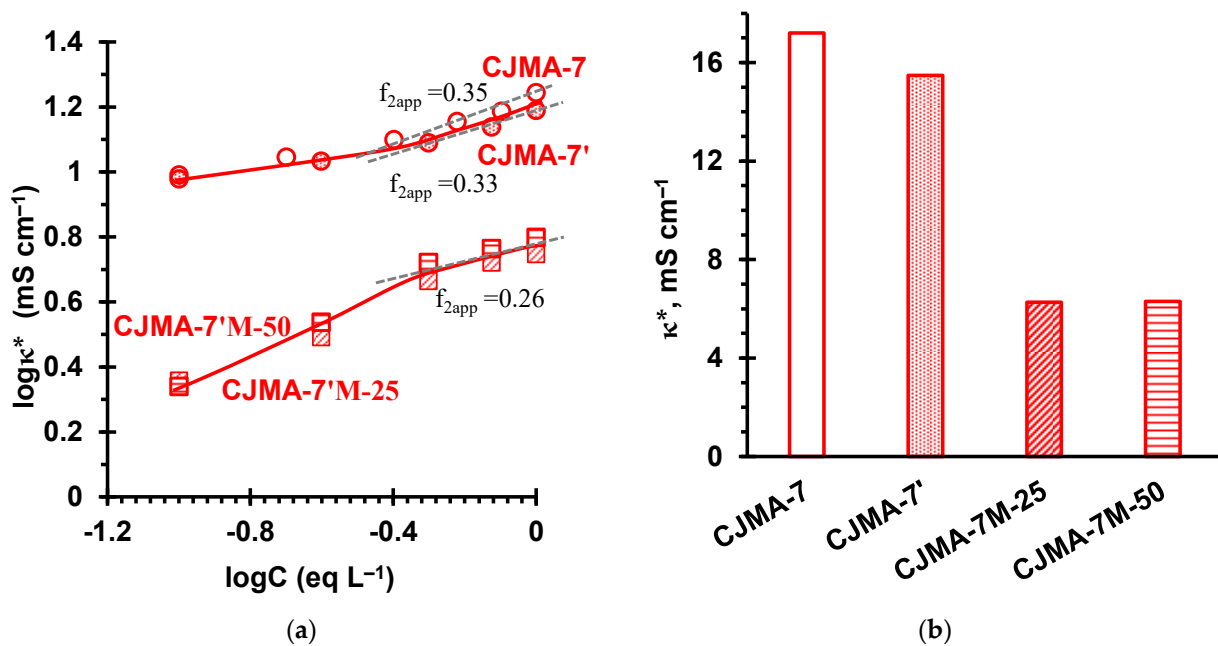


Figure 9. Concentration dependences of the electrical conductivity of the pristine membrane CJMA-7' and modified samples CJMA-7'M in NaCl solutions (a) as well as comparison of the electrical conductivity of membranes under study in 1 eq L⁻¹ NaCl (b). Indexes 25 and 50 denote the temperature (in °C) at which the modified sample was dried after casting a modifying film on its surface. The solid straight lines show the linear trend lines drawn to determine f_{2app} in the range of elevated concentrations. The solid lines are drawn to guide the eye.

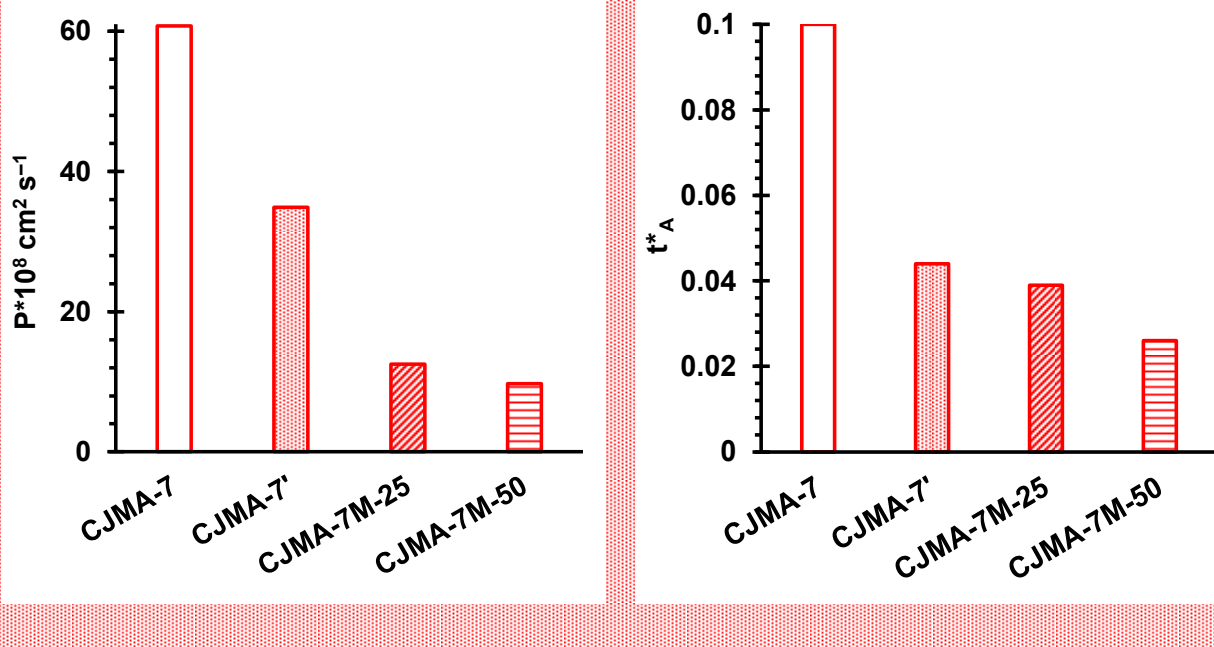


Figure 10. Diffusion permeability (a) and coion transport numbers (b) in the pristine membrane (CJMA-7) and modified samples. The data are obtained in 1.0 eq L⁻¹ NaCl solution. Indexes 25 and 50 denote the temperature (in °C) at which the modified sample was kept after casting a modifying film on its surface.

Thus, the transport number of Cl⁻ ions in the CJMA-7'M-50 membrane in 1 eq L⁻¹ NaCl is approximately equal to 0.97, which places this membrane in the counterion permselectivity between AMH-PES and AMX (Figure 7). The modifying film clogs the outlets of extended macropores on the membrane surface. As a result, the f_{2app} value found from the

concentration dependences of the electrical conductivity decreases from 0.33 (CJMA-7') to 0.28 (CJMA-7'M-25, CJMA-7'M-50). A decrease in the conductivity of the modified samples in the range of relatively high concentrations is explained by a decrease in the volume fraction of a highly conductive electrically neutral solution in the membrane due to the structural changes caused by the modification of the pristine membrane. Note that the conductivity of the modified CJMA-7'M samples in 0.1 eq L⁻¹ NaCl remains very high, about 6 mS cm⁻¹, which is approximately equal to the conductivity of AMH-PES (Figure 4) and is noticeably higher than the conductivity of AMX (4 mS cm⁻¹). The value of diffusion permeability decreased to a much greater extent (about six times, when comparing the CJMA-7 and CJMA-7M-50 membranes). The main cause is the decrease in the volume fraction of the intergel electroneutral solution, which significantly reduces the possible routes of coion transport through the membrane. A strong decrease in the diffusion permeability leads to a three-fold decrease in the coion transport number (Figure 10b).

6. Materials and Methods

6.1. Solutions

Solid NaCl and Na₂SO₄ of the analytical grade (Vecton JSC, St. Petersburg, Russia) as well as distilled water with electrical conductivity of 1.1 ± 0.1 μS cm⁻¹ and pH = 5.5 (25 °C) were used for preparation of solutions. These solutions have a pH 5.4 ± 0.3 (NaCl) and 5.6 ± 0.3 (Na₂SO₄). Some characteristics (at 25 °C) of the NaCl and Na₂SO₄ solutions as well as the ions they contain [78,79] are represented in Table S1, Supplementary Materials. Concentration dependences of NaCl [78] and Na₂SO₄ [80] diffusion coefficients (at 25 °C) normalized to the diffusion coefficient at infinite dilution solution (Table S1) are shown in Figure S1 (see Supplementary Materials).

6.2. Membrane Modification

For a year, the CJMA-7 membrane was stored in a refrigerator at a temperature of +8 °C in a 0.1 eq L⁻¹ NaCl solution (sample CJMA-7'). Then the CJMA-7' membrane was divided into two samples. A 7% solution of MF-4SK (perfluorinated sulfonated polymer in isopropyl alcohol, manufactured by Plastpolymer, Russia) [81] was poured onto the surface of each sample and dried at room temperature for 24 h until the MF-4SK film was formed (CJMA-7'M). Then these samples were dried for an additional 1 h at temperatures of 25 (sample CJMA-7'M-25) and 50 °C (sample CJMA-7'M-50) in an oven (Binder ED Avantgarde.Line, BINDER GmbH, Germany). During all the time (25 h) the CJMA-7' sample was in air at room temperature (25 °C) in order to exclude from consideration possible changes in the characteristics of CJMA-7'M-25 and CJMA-7'M-50 caused by the presence of membranes in the air.

6.3. Study of Membrane Characteristics

All studied AEMs underwent salt pretreatment before experiments [82]. The characteristics of these membranes, presented in Table 2, were found by standard methods [83], the description of which is in Supplementary Materials.

Surface and cross-section visualization of swollen AEMs was carried out with the SOPTOP CX40M optical microscope (Yuyao, Zhejiang, China) with a digital eyepiece USB camera (5×, 10×, 20×, and 50× magnification).

The AEMs electrical conductivity (κ^*) was measured by the differential method using a clip cell [84] and an immittance meter AKIP 6104 (B + K Precision Taiwan, Inc., New Taipei City, Taiwan) at an alternating current frequency of 1 kHz.

The confidence interval of the determination of the κ^* value is equal to 0.4 mS cm⁻¹.

The integral diffusion permeability coefficient of AEMs (P) was obtained using a two-compartment flow cell [85]. Supplementary Materials contain the scheme (Figure S2) of the cell, as well as the details of the measurements and data processing. The confidence interval of the determination of (P) is equal to 0.4 × 10⁻⁸ cm² s⁻¹.

7. Conclusions

In moderately dilute (0.1 eq L^{-1}) NaCl and Na_2SO_4 solutions, the counterion permselectivity of AMX, AMH-PES and CJMA-6, CJMA-3 membranes (quantified by the values of the counterion transport numbers t_1^*) is close to unity. Moreover, even in concentrated (1.0 eq L^{-1}) NaCl and Na_2SO_4 solutions, the t_1^* values for these membranes do not fall below 0.95 ± 0.01 . This means that the listed AEMs can be used both for electrodialysis desalination and concentration of electrolyte solutions.

Structural parameters provide the CJMA-6 and CJMA-3 membranes with a rather low diffusion permeability in dilute solutions, despite their relatively low exchange capacity. A feature of the CJMA-6 membrane is that it has a relatively high portion of series-connected elements of a highly selective gel phase and intergel spaces filled with an electrically neutral solution (assumed identical to the external solution). Another particularity of this membrane is its fairly dense gel phase, which is very low permeable to coions. This determines the low diffusion permeability and high counterion permselectivity of this membrane. For these characteristics, the CJMA-6 membrane is not inferior to the AMX membrane, which is considered as one of the best in the world market. In the range of relatively high concentrations (about 1 eq L^{-1}), the conductivity of the CJMA-6 membrane is approximately equal to the conductivity of AMX membrane. At the same time, in the range of low concentrations $\kappa_{\text{CJMA-6}}^* < \kappa_{\text{AMX}}^*$, which is explained by the higher exchange capacity and lower volume fraction of electroneutral solution in the AMX membrane. As for the CJMA-3 and CJMA-7 membranes, a relatively high contribution of the parallel connection of elements of the gel phase and intergel solution facilitates the electrolyte transfer through these membranes, which significantly reduces their counterion permselectivity.

The influence of the high volume fraction of the intergel solution and the contribution of the parallel connection of the gel phase and intergel solution on the diffusion permeability of CJMAED membranes is most pronounced in Na_2SO_4 solutions. This is due to two phenomena: (1) an increase in the linear dimensions of the pores of weakly crosslinked polymers due to stretching of the ion-exchange matrix when highly hydrated sulfate ions are introduced into its pores, and (2) a sharp decrease in the mobility of sulfate ions in solution with an increase in its concentration.

The CJMA-7 membrane has the lowest exchange capacity and the highest volume fraction of intergel spaces filled with the external solution. The gel phase of this membrane appears to be relatively porous, which allows both voluminous counterions and coions to pass through it. These properties determine the lowest selectivity of CJMA-7 in comparison with other investigated AEMs, which nevertheless does not fall below 0.87 ± 0.01 even in 1.0 eq L^{-1} NaCl and Na_2SO_4 solutions. It is preferable to use this membrane in the electrodialysis processing of dilute solutions, as well as for processing solutions containing large ions, for example, in the food industry.

One of the main reasons for a high diffusion permeability and low permselectivity of CJMA-7 is the presence of extended macropores, which are formed at the boundaries of ion-exchange material and the reinforcing cloth filaments. This defect is amplified when the reinforcing filaments are protruded to the membrane surface. It is shown that the CJMA-7 membrane permselectivity can be essentially improved by coating its surface with a dense homogeneous ion-exchange film.

Supplementary Materials: The following are available online at <https://www.mdpi.com/1422-0067/22/3/1415/s1>.

Author Contributions: Conceptualization, V.N. and T.X.; Methodology, N.P.; Formal Analysis, Y.W. and Y.Z.; Investigation, V.S. and V.T.; Resources, T.X. and V.N.; Writing—Original Draft Preparation, N.P.; Writing—Review and Editing, V.N., M.S., Y.W. and Y.Z.; Experimentation, V.S. and V.T.; Supervision, V.N. and N.P.; Project Administration, N.P.; Funding Acquisition, V.N. All authors have read and agreed to the published version of the manuscript.

Funding: This research was funded by Russian Foundation of Basic Researches, grant number 20-08-00933, and the National Natural Science Foundation of China, grant number 22061132003. The authors thank the Core Facility “Environmental Analytical Center” of the Kuban State University for providing their equipment.

Institutional Review Board Statement: Not applicable.

Informed Consent Statement: Not applicable.

Data Availability Statement: Not applicable.

Acknowledgments: The authors thank Ilya Moroz for obtaining optical images of the membranes.

Conflicts of Interest: The authors declare no conflict of interest.

References

1. Chu, J.Y.; Lee, K.H.; Kim, A.R.; Yoo, D.J. Improved electrochemical performance of composite anion exchange membranes for fuel cells through cross linking of the polymer chain with functionalized graphene oxide. *J. Membr. Sci.* **2020**, *611*, 118385. [[CrossRef](#)]
2. Son, T.Y.; Kim, D.J.; Vijayakumar, V.; Kim, K.; Kim, D.S.; Nam, S.Y. Anion exchange membrane using poly(ether ether ketone) containing imidazolium for anion exchange membrane fuel cell (AEMFC). *Ind. Eng. Chem. Res.* **2020**, *89*, 175–182. [[CrossRef](#)]
3. Xing, Y.; Geng, K.; Chu, X.; Wang, C.; Liu, L.; Li, N. Chemically stable anion exchange membranes based on C2-protected imidazolium cations for vanadium flow battery. *J. Membr. Sci.* **2021**, *618*, 118696. [[CrossRef](#)]
4. Jiang, Y.; Liao, J.; Yang, S.; Li, J.; Xu, Y.; Ruan, H.; Sotto, A.; Van der Bruggen, B.; Shen, J. Stable cycloaliphatic quaternary ammonium-tethered anion exchange membranes for electrodialysis. *React. Funct. Polym.* **2018**, *130*, 61–69. [[CrossRef](#)]
5. Alam, M.M.; Hossain, M.; Mei, Y.; Jiang, C.; Wang, Y.; Tang, C.Y.; Xu, T. An Alkaline stable anion exchange membrane for electro-desalination. *Desalination* **2021**, *497*, 114779. [[CrossRef](#)]
6. Kotoka, F.; Merino-Garcia, I.; Velizarov, S. Surface modifications of anion exchange membranes for an improved reverse electrodialysis process performance: A review. *Membranes* **2020**, *10*, 160. [[CrossRef](#)]
7. Golubenko, D.V.; Van der Bruggen, B.; Yaroslavtsev, A.B. Novel anion exchange membrane with low ionic resistance based on chloromethylated/quaternized-grafted polystyrene for energy efficient electromembrane processes. *J. Appl. Polym. Sci.* **2020**, *137*, 48656. [[CrossRef](#)]
8. Mikhaylin, S.; Patouillard, L.; Margni, M.; Bazinet, L. Milk protein production by a more environmentally sustainable process: Bipolar membrane electrodialysis coupled with ultrafiltration. *Green Chem.* **2018**, *20*, 449–456. [[CrossRef](#)]
9. Bdiri, M.; Perreault, V.; Mikhaylin, S.; Larchet, C.; Hellal, F.; Bazinet, L.; Dammak, L. Identification of phenolic compounds and their fouling mechanisms in ion-exchange membranes used at an industrial scale for wine tartaric stabilization by electrodialysis. *Sep. Purif. Technol.* **2020**, *233*, 115995. [[CrossRef](#)]
10. Abels, C.; Carstensen, F.; Wessling, M. Membrane processes in biorefinery applications. *J. Membr. Sci.* **2013**, *444*, 285–317. [[CrossRef](#)]
11. Bazinet, L.; Geoffroy, T.R. Electrodialytic processes: Market overview, membrane phenomena, recent developments and sustainable strategies. *Membranes* **2020**, *10*, 221. [[CrossRef](#)] [[PubMed](#)]
12. Reig, M.; Valderrama, C.; Gibert, O.; Cortina, J.L. Selectrodialysis and bipolar membrane electrodialysis combination for industrial process brines treatment: Monovalent-divalent ions separation and acid and base production. *Desalination* **2016**, *399*, 88–95. [[CrossRef](#)]
13. Zhang, Y.-F.; Liu, L.; Du, J.; Fu, R.; Van der Bruggen, B.; Zhang, Y. Fracsis: Ion fractionation and metathesis by a NF-ED integrated system to improve water recovery. *J. Membr. Sci.* **2017**, *523*, 385–393. [[CrossRef](#)]
14. Ahmed, F.E.; Hashaikeh, R.; Hilal, N. Hybrid technologies: The future of energy efficient desalination—A review. *Desalination* **2020**, *495*, 114659. [[CrossRef](#)]
15. Rotta, E.H.; Bitencourt, C.S.; Marder, L.; Bernardes, A.M. Phosphorus recovery from low phosphate-containing solution by electrodialysis. *J. Membr. Sci.* **2019**, *573*, 293–300. [[CrossRef](#)]
16. Abou-Shady, A. Recycling of polluted wastewater for agriculture purpose using electrodialysis: Perspective for large scale application. *Chem. Eng. Trans.* **2017**, *323*, 1–18. [[CrossRef](#)]
17. Shi, L.; Xie, S.; Hu, Z.; Wu, G.; Morrison, L.; Croot, P.; Hu, H.; Zhan, X. Nutrient recovery from pig manure digestate using electrodialysis reversal: Membrane fouling and feasibility of long-term operation. *J. Membr. Sci.* **2019**, *573*, 560–569. [[CrossRef](#)]
18. Zhao, Y.; Tang, K.; Liu, H.; Van der Bruggen, B.; Sotto Díaz, A.; Shen, J.; Gao, C. An anion exchange membrane modified by alternate electro-deposition layers with enhanced monovalent selectivity. *J. Membr. Sci.* **2016**, *520*, 262–271. [[CrossRef](#)]
19. Golubenko, D.; Yaroslavtsev, A. Development of surface-sulfonated graft anion-exchange membranes with monovalent ion selectivity and antifouling properties for electromembrane processes. *J. Membr. Sci.* **2020**, *612*, 118408. [[CrossRef](#)]
20. Lejarazu-Larrañaga, A.; Zhao, Y.; Molina, S.; García-Calvo, E.; Van der Bruggen, B. Alternating current enhanced deposition of a monovalent selective coating for anion exchange membranes with antifouling properties. *Sep. Purif. Technol.* **2019**, *229*, 115807. [[CrossRef](#)]

21. Bdiri, M.; Dammak, L.; Larchet, C.; Hellal, F.; Porozhnyy, M.; Nevakshenova, E.; Pismenskaya, N.; Nikonenko, V. Characterization and cleaning of anion-exchange membranes used in electrodialysis of polyphenol-containing food industry solutions; comparison with cation-exchange membranes. *Sep. Purif. Technol.* **2019**, *210*, 636–650. [CrossRef]
22. Doi, S.; Takumi, N.; Kakihana, Y.; Higa, M. Alkali attack on cation-exchange membranes with polyvinyl chloride backing and binder: Comparison with anion-exchange membranes. *Membranes* **2020**, *10*, 228. [CrossRef] [PubMed]
23. Zhou, J.; Kuang, H.; Zhuang, W.; Chen, Y.; Liu, D.; Ying, H.; Wu, J. Application of electrodialysis to extract 5'-ribonucleotides from hydrolysate: Efficient decolorization and membrane fouling. *RSC Adv.* **2018**, *8*, 29115–29128. [CrossRef]
24. Nugraha, A.F.; Arbi, M.R.; Wijaya, F.; Lee, H.; Shin, D.; Bae, B. Synthesis and characterization of anion-exchange multi-block-copolymer membranes containing highly densified cationic functional groups. *Polymer* **2020**, *210*, 122996. [CrossRef]
25. Du, X.; Wang, Z.; Zhang, H.; Yuan, Y.; Wang, H.; Zhang, Z. Prepared poly(aryl piperidinium) anion exchange membranes for acid recovery to improve dialysis coefficients and selectivity. *J. Membr. Sci.* **2021**, *619*, 118805. [CrossRef]
26. Yu, S.; Zhu, J.; Liao, J.; Ruan, H.; Sotto, A.; Shen, J. Homogeneous trimethylamine-quaternized polysulfone-based anion exchange membranes with crosslinked structure for electrodialysis desalination. *Sep. Purif. Technol.* **2021**, *257*, 117874. [CrossRef]
27. Cavaliere, S.; Subianto, S.; Savych, I.; Jones, D.J.; Rozière, J. Electrospinning: Designed architectures for energy conversion and storage devices. *Energy Environ. Sci.* **2011**, *4*, 4761. [CrossRef]
28. Di Vona, M.L.; Knauth, P. Electrochemical synthesis of ion exchange polymers: Comparison between hydroxide and proton conductors. *Solid State Ion.* **2020**, *352*, 115370. [CrossRef]
29. Ohashi, H.; Jung, H.; Chi, X.; Miyanishi, S.; Yamaguchi, T. Alkali-resistant anion exchange membranes with grafted polyelectrolyte for fuel cells. *Chem. Lett.* **2018**, *47*, 857–859. [CrossRef]
30. Ran, J.; Wu, L.; He, Y.; Yang, Z.; Wang, Y.; Jiang, C.; Ge, L.; Bakangura, E.; Xu, T. Ion exchange membranes: New developments and applications. *J. Membr. Sci.* **2017**, *522*, 267–291. [CrossRef]
31. Wang, Y.; Zhang, Z.; Jiang, C.; Xu, T. Recovery of gamma-aminobutyric acid (GABA) from reaction mixtures containing salt by electrodialysis. *Sep. Purif. Technol.* **2016**, *170*, 353–359. [CrossRef]
32. Wei, X.; Wang, Y.; Yan, H.; Wu, K.; Xu, T. Purification of methylsulfonylmethane from mixtures containing salt by conventional electrodialysis. *Membranes* **2020**, *10*, 23. [CrossRef] [PubMed]
33. Peng, C.; Liu, H.; Qiao, H.; Luo, J.; Liu, X.; Hou, R.; Wan, X.; Cai, H. Evaluation of the feasibility of short-term electrodialysis for separating naturally occurring fluoride from instant brick tea infusion. *J. Sci. Food Agric.* **2020**, *100*, 168–176. [CrossRef] [PubMed]
34. Li, W.; Wang, J.; Nie, Y.; Wang, D.; Xu, H.; Zhang, S. Separation of soluble saccharides from the aqueous solution containing ionic liquids by electrodialysis. *Sep. Purif. Technol.* **2020**, *251*, 117402. [CrossRef]
35. Berkessa, Y.W.; Lang, Q.; Yan, B.; Kuang, S.; Mao, D.; Shu, L.; Zhang, Y. Anion exchange membrane organic fouling and mitigation in salt valorization process from high salinity textile wastewater by bipolar membrane electrodialysis. *Desalination* **2019**, *465*, 94–103. [CrossRef]
36. Yan, H.; Wang, Y.; Wu, L.; Shehzad, M.A.; Jiang, C.; Fu, R.; Liu, Z.; Xu, T. Multistage-batch electrodialysis to concentrate high-salinity solutions: Process optimisation, water transport, and energy consumption. *J. Membr. Sci.* **2019**, *570–571*, 245–257. [CrossRef]
37. Zhou, Y.; Yan, H.; Wang, X.; Wu, L.; Wang, Y.; Xu, T. Electrodialytic concentrating lithium salt from primary resource. *Desalination* **2018**, *425*, 30–36. [CrossRef]
38. Zabolotsky, V.I.; Nikonenko, V.V. Effect of structural membrane inhomogeneity on transport properties. *J. Membr. Sci.* **1993**, *79*, 181–198. [CrossRef]
39. Manohar, M.; Thakur, A.K.; Pandey, R.P.; Shahi, V.K. Efficient and Stable Anion exchange membrane: Tuned membrane permeability and charge density for molecular/ionic separation. *J. Membr. Sci.* **2015**, *496*, 250–258. [CrossRef]
40. Sedkaoui, Y.; Szymczyk, A.; Lounici, H.; Arous, O. A new lateral method for characterizing the electrical conductivity of ion-exchange membranes. *J. Membr. Sci.* **2016**, *507*, 34–42. [CrossRef]
41. Kedem, O.; Katchalsky, A. Permeability of composite membranes. Part 3—Series array of elements. *Trans. Faraday Soc.* **1963**, *59*, 1941–1953. [CrossRef]
42. Gnusin, N.P.; Berezina, N.P.; Shudrenko, A.A.; Ivina, A.P. Electrolyte diffusion across ion-exchange membranes. *Russ. J. Phys. Chem. A* **1994**, *68*, 506–510.
43. Gnusin, N.P.; Ivina, O.P. Diffusion of sodium chloride through an MK-40 cation-exchange membrane. *Russ. J. Phys. Chem.* **1991**, *65*, 1299–1303.
44. Larchet, C.; Dammak, L.; Auclair, B.; Parchikov, S.; Nikonenko, V. A simplified procedure for ion-exchange membrane characterisation. *New J. Chem.* **2004**, *28*, 1260. [CrossRef]
45. Garcia-Vasquez, W.; Ghalloussi, R.; Dammak, L.; Larchet, C.; Nikonenko, V.; Grande, D. Structure and properties of heterogeneous and homogeneous ion-exchange membranes subjected to ageing in sodium hypochlorite. *J. Membr. Sci.* **2014**, *452*, 104–116. [CrossRef]
46. Website of Hefei ChemJoy Polymer Materials Co., Ltd. Available online: <http://www.cj-membrane.com/display/369191.html> (accessed on 4 July 2020).
47. Yan, H.; Wang, Y.; Xu, T. Developing Ion Exchange Membrane for Treating High Salinity Water Using Electrodialysis. In Proceedings of the 5th international conferences on Sustainable Chemical Product and Process Engineering (SCPPE), Tianjin, China, 30 July 2019. Abstract Number K6-5, 65–67.

48. Mizutani, Y.; Yamane, R.; Ihara, H.; Motomura, H. Studies of ion exchange membranes. XVI. The preparation of ion exchange membranes by the “paste method”. *Bull. Chem. Soc. Jpn.* **1963**, *36*, 361–366. [[CrossRef](#)]
49. Hori, Y.; Nakatani, T.; Mizutani, Y. Morphology of ion exchange membranes. *J. Electron Microsc.* **1986**, *35*, 220–226. [[CrossRef](#)]
50. Website of MEGA, a.s. Available online: <https://www.mega.cz/membranes/> (accessed on 26 December 2020).
51. Bulejko, P.; Stránská, E.; Weinertová, K. Electrochemical and mechanical stability of ion-exchange membranes in alkaline solution. *Chem. Pap.* **2017**, *71*, 1303–1309. [[CrossRef](#)]
52. Melnikov, S.; Shkirskaia, S. Transport properties of bilayer and multilayer surface-modified ion-exchange membranes. *J. Membr. Sci.* **2019**, *590*, 117272. [[CrossRef](#)]
53. Güler, E.; van Baak, W.; Saakes, M.; Nijmeijer, K. Monovalent-ion-selective membranes for reverse electrodialysis. *J. Membr. Sci.* **2014**, *455*, 254–270. [[CrossRef](#)]
54. Mareev, S.A.; Butylskii, D.Y.; Pismenskaya, N.D.; Larchet, C.; Dammak, L.; Nikonenko, V.V. Geometric heterogeneity of homogeneous ion-exchange neosepta membranes. *J. Membr. Sci.* **2018**, *563*, 768–776. [[CrossRef](#)]
55. Pismenskaya, N.; Sarapulova, V.; Nevakshenova, E.; Kononenko, N.; Fomenko, M.; Nikonenko, V. Concentration dependencies of diffusion permeability of anion-exchange membranes in sodium hydrogen carbonate, monosodium phosphate, and potassium hydrogen tartrate solutions. *Membranes* **2019**, *9*, 170. [[CrossRef](#)] [[PubMed](#)]
56. Akberova, E.M.; Vasil'eva, V.I.; Zabolotsky, V.I.; Novak, L. A Study of ralex membrane morphology by SEM. *Membranes* **2019**, *9*, 169. [[CrossRef](#)] [[PubMed](#)]
57. Lide, D.R. *CRC Handbook of Chemistry and Physics*, 84th ed.; CRC Press: Boca Raton, FL, USA, 2003.
58. Rijnaarts, T.; Moreno, J.; Saakes, M.; de Vos, W.M.; Nijmeijer, K. Role of anion exchange membrane fouling in reverse electrodialysis using natural feed waters. *Colloids Surf. A Phys. Eng. Asp.* **2019**, *560*, 198–204. [[CrossRef](#)]
59. Jiang, C.; Wang, Y.; Zhang, Z.; Xu, T. Electrodialysis of concentrated brine from RO plant to produce coarse salt and freshwater. *J. Membr. Sci.* **2014**, *450*, 323–330. [[CrossRef](#)]
60. Le, X.T. Permselectivity and microstructure of anion exchange membranes. *J. Colloid Interface Sci.* **2008**, *325*, 215–222. [[CrossRef](#)]
61. Lee, H.-J.; Hong, M.-K.; Han, S.-D.; Cho, S.-H.; Moon, S.-H. Fouling of an anion exchange membrane in the electrodialysis desalination process in the presence of organic foulants. *Desalination* **2009**, *238*, 60–69. [[CrossRef](#)]
62. Jaroszek, H.; Dydo, P. Potassium nitrate synthesis by electrodialysis-metathesis: The effect of membrane type. *J. Membr. Sci.* **2018**, *549*, 28–37. [[CrossRef](#)]
63. Vermaas, D.A.; Veerman, J.; Saakes, M.; Nijmeijer, K. Influence of multivalent ions on renewable energy generation in reverse electrodialysis. *Energy Environ. Sci.* **2014**, *7*, 1434–1445. [[CrossRef](#)]
64. Melnikov, S.; Loza, S.; Sharafan, M.; Zabolotskiy, V. Electrodialysis treatment of secondary steam condensate obtained during production of ammonium nitrate. Technical and economic analysis. *Sep. Purif. Technol.* **2016**, *157*, 179–191. [[CrossRef](#)]
65. Güler, E.; Elizen, R.; Vermaas, D.A.; Saakes, M.; Nijmeijer, K. Performance-determining membrane properties in reverse electrodialysis. *J. Membr. Sci.* **2013**, *446*, 266–276. [[CrossRef](#)]
66. Kozaderova, O.A.; Kim, K.B.; Niftaliev, S.I. Changes of physicochemical and transport characteristics of ion exchange membranes in the process of operation under demineralization of wastewater production of nitrogen-containing mineral fertilizers. *Sorpt. Chromatogr. Process.* **2018**, *18*, 875–885. [[CrossRef](#)]
67. Zabolotskii, V.I.; Mel'nikov, S.S.; Demina, O.A. Prediction of the mass exchange characteristics of industrial electrodialyzer concentrators. *Russ. J. Electrochem.* **2014**, *50*, 32–37. [[CrossRef](#)]
68. Ren, M.; Ning, P.; Xu, J.; Qu, G.; Xie, R. Concentration and treatment of ceric ammonium nitrate wastewater by integrated electrodialysis-vacuum membrane distillation process. *Chem. Eng. J.* **2018**, *351*, 721–731. [[CrossRef](#)]
69. Zhang, N.; Liu, Y.; Liu, R.; She, Z.; Tan, M.; Mao, D.; Fu, R.; Zhang, Y. Polymer inclusion membrane (PIM) containing ionic liquid as a proton blocker to improve waste acid recovery efficiency in electrodialysis process. *J. Membr. Sci.* **2019**, *581*, 18–27. [[CrossRef](#)]
70. Yan, H.; Xu, C.; Li, W.; Wang, Y.; Xu, T. Electrodialysis to concentrate waste ionic liquids: Optimization of operating parameters. *Ind. Eng. Chem. Res.* **2016**, *55*, 2144–2152. [[CrossRef](#)]
71. Sarapulova, V.; Shkorkina, I.; Mareev, S.; Pismenskaya, N.; Kononenko, N.; Larchet, C.; Dammak, L.; Nikonenko, V. Transport characteristics of Fujifilm ion-exchange membranes as compared to homogeneous membranes AMX and CMX and to heterogeneous membranes MK-40 and MA-41. *Membranes* **2019**, *9*, 84. [[CrossRef](#)]
72. Helfferich, F.G. *Ion Exchange*; McGraw-Hill: New York, NY, USA, 1962; ASIN: B0000CLGWI.
73. Kamcev, J.; Paul, D.R.; Freeman, B.D. Equilibrium ion partitioning between aqueous salt solutions and inhomogeneous ion exchange membranes. *Desalination* **2018**, *446*, 31–41. [[CrossRef](#)]
74. Zhu, S.; Kingsbury, R.S.; Call, D.F.; Coronell, O. Impact of solution composition on the resistance of ion exchange membranes. *J. Membr. Sci.* **2018**, *554*, 39–47. [[CrossRef](#)]
75. Demina, O.A.; Kononenko, N.A.; Falina, I.V.; Demin, A.V. Theoretical estimation of differential coefficients of ion-exchange membrane diffusion permeability. *Colloid J.* **2017**, *79*, 317–327. [[CrossRef](#)]
76. Sarapulova, V.V.; Titorova, V.D.; Nikonenko, V.V.; Pismenskaya, N.D. Transport characteristics of homogeneous and heterogeneous ion-exchange membranes in sodium chloride, calcium chloride, and sodium sulfate solutions. *Membr. Membr. Technol.* **2019**, *1*, 168–182. [[CrossRef](#)]

77. Alberti, G.; Narducci, R.; Sganappa, M. Effects of hydrothermal/thermal treatments on the water-uptake of nafion membranes and relations with changes of conformation, counter-elastic force and tensile modulus of the matrix. *J. Power Sources* **2008**, *178*, 575–583. [CrossRef]
78. Robinson, R.A.; Stokes, R.H. *Electrolyte Solutions*, 2nd rev. ed.; Dover Publications: Mineola, NY, USA, 2002; ISBN 978-0-486-42225-1.
79. Luo, T.; Abdu, S.; Wessling, M. Selectivity of ion exchange membranes: A review. *J. Membr. Sci.* **2018**, *555*, 429–454. [CrossRef]
80. Rard, J.A.; Miller, D.G. The Mutual diffusion coefficients of NaCl-H₂O and CaCl₂-H₂O at 25 °C from rayleigh interferometry. *J. Solut. Chem.* **1979**, *8*, 701–716. [CrossRef]
81. Website of PlastPolymer JSC. Available online: <http://www.plastpolymer.com/structure/otdel-politetraftorjetilena-i-perftorirovannyh-ionoobmennyh-membran/> (accessed on 27 December 2020).
82. Berezina, N.P.; Kononenko, N.A.; Dyomina, O.A.; Gnusin, N.P. Characterization of ion-exchange membrane materials: Properties vs structure. *Adv. Colloid Interface Sci.* **2008**, *139*, 3–28. [CrossRef]
83. Nagarale, R.K.; Gohil, G.S.; Shahi, V.K. Recent developments on ion-exchange membranes and electro-membrane processes. *Adv. Colloid Interface Sci.* **2006**, *119*, 97–130. [CrossRef]
84. Lteif, R.; Dammak, L.; Larchet, C.; Auclair, B. Conductivité électrique membranaire: Étude de l'effet de la concentration, de la nature de l'électrolyte et de la structure membranaire. *Eur. Polym. J.* **1999**, *35*, 1187–1195. [CrossRef]
85. Pismenskaya, N.D.; Nevakshenova, E.E.; Nikonenko, V.V. Using a single set of structural and kinetic parameters of the micro-heterogeneous model to describe the sorption and kinetic properties of ion-exchange membranes. *Pet. Chem.* **2018**, *58*, 465–473. [CrossRef]